ELSEVIER

Journal of Alloys and Compounds 317–318 (2001) 428–432

Journal of ALLOYS AND COMPOUNDS

www.elsevier.com/locate/jallcom

Theoretical study of structural stability and magnetism in the Pd_3Mn antiphase

Janusz Tobola[a,b,*], Pierre Pécheur[a]

[a]*Laboratoire de Physique des Matériaux, Ecole des Mines, Parc du Saurupt, 54042 Nancy Cédex, France*
[b]*Faculty of Physics and Nuclear Techniques, University of Mining and Metallurgy, Al. Mickiewicza 30, 30-059 Kraków, Poland*

Abstract

Relative stability of $L1_2$, DO_{22} and DO_{23} structures as well as magnetic properties are studied in the Pd_3Mn antiferromagnet using the Korringa–Kohn–Rostoker band structure calculations within the local-spin-density approach. The DO_{23} phase of Pd_3Mn is found to be the most stable from the total energy analysis if accounting for the spin-polarisation. The equilibrium lattice constant in DO_{23} lies between a_{eq} of the $L1_2$ and DO_{22} phases, being about 1% larger than the experimental value. Noteworthy, the total energies of the ferromagnetic DO_{22} and DO_{23} phases of Pd_3Mn markedly approach, when going down to the experimental lattice constant. In ferromagnetic state of Pd_3Mn the following magnetic moments (in μ_B) 4.08, 0.12, 0.16 and 0.15 are computed on Mn and 4*c*, 4*d* and 4*e* sites of Pd, respectively. In antiferromagnetic state, albeit no magnetic moment on Pd (4*d*), the KKR values are close to the ferromagnetic results, namely (in μ_B) 3.99 on Mn, 0.18 on Pd (4*c*) and 0.16 on Pd (4*e*). The electronic structure and magnetic properties of Pd_3V and Pd_3Fe in the $L1_2$, DO_{22} phases are also reported. The KKR calculations show that the ground state of Pd_3V is either magnetic ($L1_2$) or non-magnetic (DO_{22}). Conversely, Pd_3Fe exhibits ferromagnetic properties in both crystal structures with the Fe and Pd magnetic moments (in μ_B) 3.28, 0.29 and 3.22, 0.22, 0.26 in $L1_2$ and DO_{22}, respectively. Both structural and magnetic properties derived from the band structure KKR calculations generally correspond well to the experimental data.

Keywords: Band structure; KKR method; Palladium compounds; Magnetic properties; Total energy calculations; Structural stability

1. Introduction

It is known that the Pd_3Mn compound, unlike other Pd_3T systems (T=3d element), crystallises in the long-range tetragonal 'antiphase' DO_{23} structure ($ZrAl_3$-type, SG: *I*4/*mmm*) [1] with the lattice parameters close to the ideal ratio $c/a=4$. This phase (Fig. 1) is a crystallographic combination of a simple cubic $L1_2$ structure (Cu_3Al-type, SG: *Pm*3*m*) and a tetragonal body-centred DO_{22} structure (Al_3Ti-type, SG: *I*4*mm*), observed in other Pd_3T systems. A long-range distortion occurring in $Pd_{1-x}Mn_x$ at $x\approx0.25$ was first interpreted using a nearly free electron concept of 'accommodating' of the Fermi surface to the Brillouin-zone boundaries [2]. The relative stability of the $L1_2$, DO_{22} and DO_{23} structures, in view of the band theory, has been primarily studied in the transition metal aluminides MAl_3 [3,4]. As far as Pd_3Mn is concerned, earlier electronic structure calculations were performed for the cubic structure by the non-self consistent OLCAO method [5] and the self-consistent LMTO method [6] but without including the spin-polarisation. However, both methods correctly predicted a magnetic ordering in Pd_3Mn taking into account density of states at the Fermi energy $N(E_F)$ and the

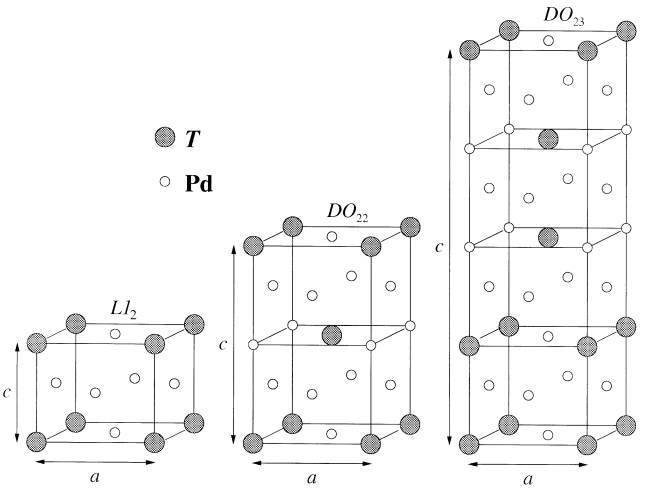

Fig. 1. Crystal structure of the $L1_2$, DO_{22} and DO_{23} phases of Pd_3T compounds. Open and grey circles represents Pd and *T* atoms, respectively.

*Corresponding author. Tel.: +48-12-6172321; fax: +48-12-6340010.
E-mail address: tobola@ftj.agh.edu.pl (J. Tobola).

0925-8388/01/$ – see front matter
PII: S0925-8388(00)01421-3

Table 1
Crystallographic positions occupied by Pd and T atoms in the $L1_2$, DO_{22}, DO_{23} phases of Pd_3T ($z_{Pd}=0.375$ and $z_{Mn}=0.125$ are used in the KKR study of the Pd_3Mn antiphase)

	$L1_2$	DO_{22}	DO_{23}
Pd	3*c*: 0, $^1/_2$, $^1/_2$	2*b*: 0, 0, $^1/_2$	4*c*: 0, $^1/_2$, 0; $^1/_2$, 0, 0
		4*d*: 0, $^1/_2$, $^1/_4$	4*d*: 0, $^1/_2$, $^1/_4$; $^1/_2$, 0, $^1/_4$
			4*e*: 0, 0, z_{Pd}; 0, 0, $-z_{Pd}$
T	1*a*: 0, 0, 0	2*a*: 0, 0, 0	4*e*: 0, 0, z_T; 0, 0, $-z_T$

Stoner parameters. Recently, the influence of spin-polarisation on selection of crystallographic structure type ($L1_2$ or DO_{22}) in Pd_3T (T=3d element) have been examined by the sophisticated LAPW calculations [7,8]. The total energy analysis clearly revealed, that the spin-polarisation was crucial to determine accurately ground state crystal structures for the Pd_3T compounds. Noteworthy, the DO_{23} structure of Pd_3Mn was not considered in the previous theoretical works. This inspired us to investigate electronic structure and magnetic properties of Pd_3Mn in a systematic way, within the $L1_2$, DO_{22} and DO_{23} phases, using the Korringa–Kohn–Rostoker (KKR) method [9,10] and the local-spin-density (LSD) approximation. Furthermore, we report the electronic structure and magnetism in Pd_3V and Pd_3Fe considering both $L1_2$ and DO_{22} structures, making a comparison with the titled compound.

2. Computational details

We have carried out fully charge and spin self-consistent KKR computations on Pd_3Mn within the $L1_2$, DO_{22} and DO_{23} phases as well as on Pd_3Fe and Pd_3V in the $L1_2$ and DO_{22} phases. The Pd and T atoms occupy the crystallographic sites in the above-mentioned structures as listed in Table 1. The total energy KKR study was done in the muffin–tin (MT) geometry as follows: non-overlapping MT radii were assumed to be equal for Pd and Mn atoms, resulting in a packing ratio ($\Sigma V^i_{MT}/V_{WS}$) near 74%; the c lattice parameter was changed coherently with a, fixing the ratio of $c/a=2$ and $c/a=4$, in DO_{22} and DO_{23}, respectively. The experimental lattice parameters [11] measured in the Pd_3T compounds (Table 2) justify using the ideal value of c/a in our electronic structure calculations. The self-consistent cycles were repeated until maximum difference between input–output potentials was less than 1 mRy. For the final potentials (the exchange-correlation part of the Barth–Hedin form [12]) total, site- and l-decomposed ($l_{max}=2$) DOS were computed on a 601 energy point mesh using a tetrahedral **k**–space integration technique [13]. Moreover, from the spin-polarised calculations, accounting for ferromagnetic and/or antiferromagnetic ordering, magnetic moments per Wigner–Seitz cell as well as per MT sphere were computed in the Pd_3T (T=V, Mn and Fe) compounds. Despite the equilibrium, lattice parameters were deduced from the total energy parabola for the three mentioned structures; all DOS spectra and magnetic moment values, presented here, correspond to the KKR results obtained at the experimental lattice constants.

Table 2
The experimental lattice parameter a and c/a in Pd_3T (T=V, Mn, Fe) [11][a]

	Pd_3V (DO_{22})	Pd_3Mn (DO_{23})	Pd_3Fe ($L1_2$)
a (Å)	3.847	3.913	3.848
c/a	2.01 (2)	3.96 (4)	1

[a] Ideal c/a ratio is given in parenthesis.

3. Results and discussion

3.1. Structural stability

Fig. 2 shows non-polarised DOS in the three structures of the Pd_3Mn compound. At first sight, we conclude that

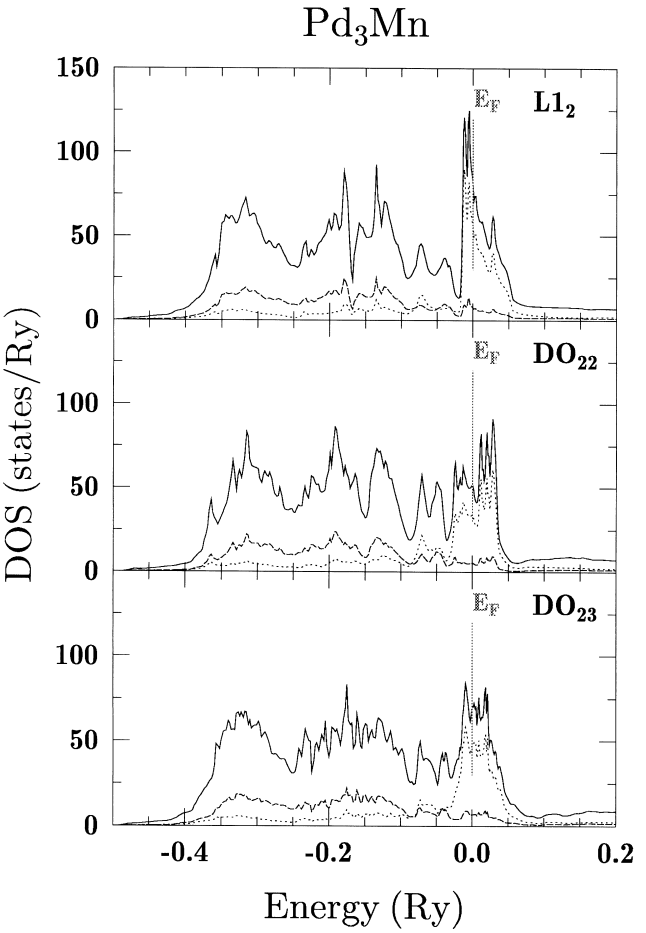

Fig. 2. Non-polarised KKR density of states in the Pd_3Mn phases. Solid, dotted and dashed lines show total, Mn and Pd (average) DOS contributions, respectively (E_F is at zero).

density of states in the vicinity of E_F is markedly increased in the $L1_2$ cubic structure unlike the tetragonal body-centred DO_{22} and DO_{23} phases. Generally, we notice that the conduction band is formed basically from d-states on Mn, being highly peaked in the vicinity of E_F, and on Pd, constituting mostly lower lying bands. Peculiarly, some features on DOS in the antiphase structure can be related to the DOS characteristics found in the simple cubic and tetragonal-body centred structures. A large d-like peak of Mn–DOS found in the $L1_2$ phase also appears, but is less pronounced, in the antiphase Pd_3Mn. Looking at $N(E_F)$ values (in parenthesis in states/Ry/spin/f.u.) in the $L1_2$ (80.5), DO_{22} (52.0) and DO_{23} (70.1) phases, as well as at centres of gravity of the conduction band, one concludes that the antiphase is not predicted correctly as the most stable structure of Pd_3Mn (at T = 0 K). This prompted us to perform the total energy spin-polarised KKR computations (in ferromagnetic state) at three lattice parameters a in the above-mentioned crystal phases of Pd_3Mn. From the lowest lying $E_{tot}(a)$ parabola (Fig. 3), corresponding to the antiphase structure, we deduce the equilibrium lattice constant $a_{eq} = 3.94$ Å. The theoretical value remains in fair agreement with the experimental value $a_{exp} = 3.913$ Å [11]. Interestingly, the a_{eq} value gained in DO_{23} lies between the corresponding a_{eq} obtained in the simple cubic (3.95 Å) and tetragonal body-centred structures (3.90 Å). Notably, at the experimental lattice constant the total energies $E_{tot}(DO_{23})$ and $E_{tot}(DO_{22})$ are found very close. If analysing in detail contributions to the total energy in these two structures, no particular differences are noticed as far as the band term E_{band} is concerned (unlike the $L1_2$ phase). Hence, the preference of the antiphase structure in Pd_3Mn is mainly due to a subtle balance between potential and kinetic contributions, which are rather different in the DO_{22} and DO_{23} phases. Interestingly, from the KKR computations of the Pd_3Mn in antiferromagnetic state, we see that all contributions to the total energy slightly decrease in respect to the ferromagnetic state ($\delta E \approx 8$ mRy). Besides, the $E_{tot}(a)$ functions in the DO_{22} and DO_{23} structures display rather close curvatures, which indicates close values of bulk modulus, unlike the $L1_2$ phase.

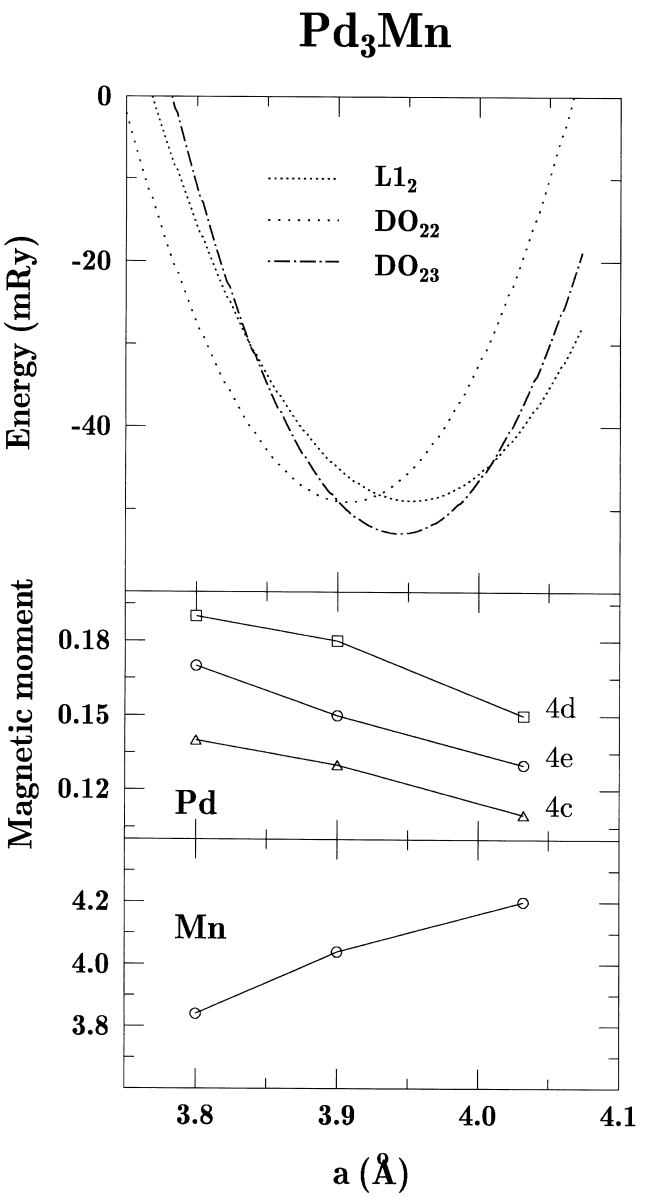

Fig. 3. Total energy parabola in the $L1_2$, DO_{22} ($c/a = 2$) and DO_{23} ($c/a = 4$) phases of Pd_3Mn derived from the KKR method. Below, lattice constant variations of Mn and Pd magnetic moments (in μ_B) for the DO_{23} phase.

In Fig. 4 the non-polarised DOS for Pd_3V and Pd_3Fe both in the $L1_2$ and DO_{22} phases are presented. It seems intriguing that the $P = N(DO_{22})/N(L1_2)|_{E_F}$ factor, defined as a ratio of DOS values at the Fermi energy in the DO_{22} and $L1_2$ structures, increases in systematic way when filling d-like states in the Pd_3T compounds. Thus, when passing from Pd_3V through Pd_3Mn to Pd_3Fe, P reaches values of 0.24, 0.64 and 1.01, respectively. These ratios remain in agreement with the previous LAPW study [7] ($P = 0.32$, 0.63 and 1.06).

3.2. Magnetic properties

From experiment, the Pd_3V (DO_{22}), Pd_3Mn (DO_{23}) and Pd_3Fe ($L1_2$) compounds show paramagnetic, antiferromagnetic and ferromagnetic properties, respectively.

The total and site-decomposed DOS in the ferromagnetic Pd_3Mn derived from the spin-polarised KKR calculations is shown in Fig. 5. We observe that d-states on Mn are almost completely polarised, giving a large magnetic moment (4.08 μ_B). Consequently, the low $N(E_F)$ is seen on Mn site both for up- and down-spin electrons. On the other hand, the Fermi level lies on the slope of d-states on Pd, which significantly increases $N(E_F)$. Slightly different values of magnetic moments computed on all Pd sites (Table 3), reflect subtle modifications of the respective

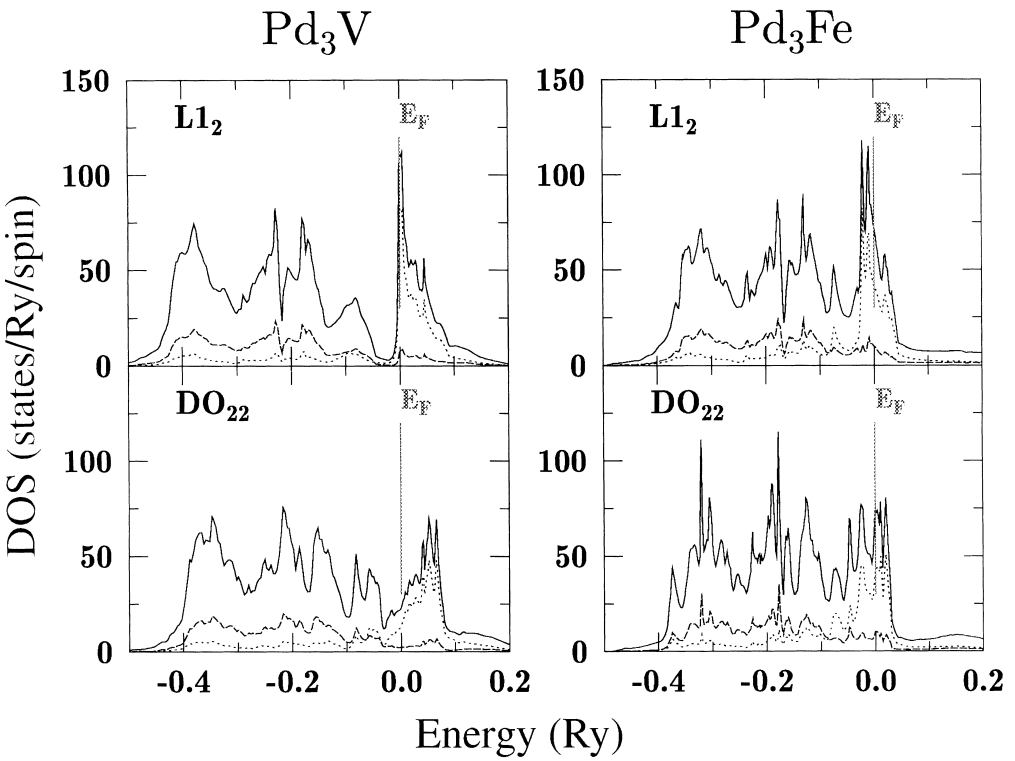

Fig. 4. Non-polarised KKR density of states in the $L1_2$ and DO_{22} phases of Pd_3V and Pd_3Fe. Total DOS is given in states/Ry/spin/f.u. Solid, dotted and dashed lines show total, T and Pd (average) DOS contributions, respectively (E_F is at zero).

Pd–DOS (Fig. 5). Note, that in the considered phases of Pd_3Mn, both palladium and manganese atoms have identical nearest neighbours in the first shell, namely Pd (8 Pd+4 Mn) and Mn (12 Pd). Thus, some changes of electronic structure and magnetic properties observed in the $L1_2$, DO_{22}, DO_{23} structures correspond to the next nearest neighbours effects. Furthermore, from the calculations in Pd_3Mn at various lattice constants, we conclude that μ_{Mn} and μ_{Pd} vary in opposite ways when a increases (Fig. 3).

In the antiferromagnetic state computations a magnetic cell as refined in Ref. [1] has been taken into account. Thus the tetragonal body-centred symmetry is no more valid, and the tetragonal simple structure has been used. The magnetic moment on Mn (3.99 μ_B) is close to the value computed in the FM state (Table 3). However, the Pd magnetic moments 0.18 μ_B and 0.16 μ_B are observed only on the (4*c*) and (4*e*) sites, unlike the (4*d*) one, being cancelled due to the symmetry of surrounding μ_{Mn}. Our KKR results remain in excellent agreement with the earlier

Table 3
Magnetic moments and DOS at E_F (in states/Ry/spin/f.u.) Pd_3T (T=V, Mn, Fe) derived from the spin-polarised KKR method[a]

	Pd_3V		Pd_3Mn			Pd_3Fe	
	$L1_2$	DO_{22}	$L1_2$	DO_{22}	DO_{23}	$L1_2$	DO_{22}
μ_{Pd}	−0.03	0	0.11	2*b*: 0.22 4*d*: 0.21	4*c*: 0.12 (0.18) 4*d*: 0.16 (0) 4*e*: 0.15 (0.16)	0.29	2*b*: 0.22 4*d*: 0.26
μ_T	1.34	0	3.98	4.08	4.03 (3.99)	3.25	3.22
μ_{tot}	1.29	0	4.35	4.80	4.51 (0)	4.07	3.93
$N_+(E_F)$	72.5	23.3	29.1	10.4	21.3 (26.1)	9.2	6.7
$N_-(E_F)$	3.8	23.3	29.4	24.3	28.1 (26.1)	36.6	28.2

[a] The antiferromagnetic results for Pd_3Mn (DO_{23}) are given in parenthesis.

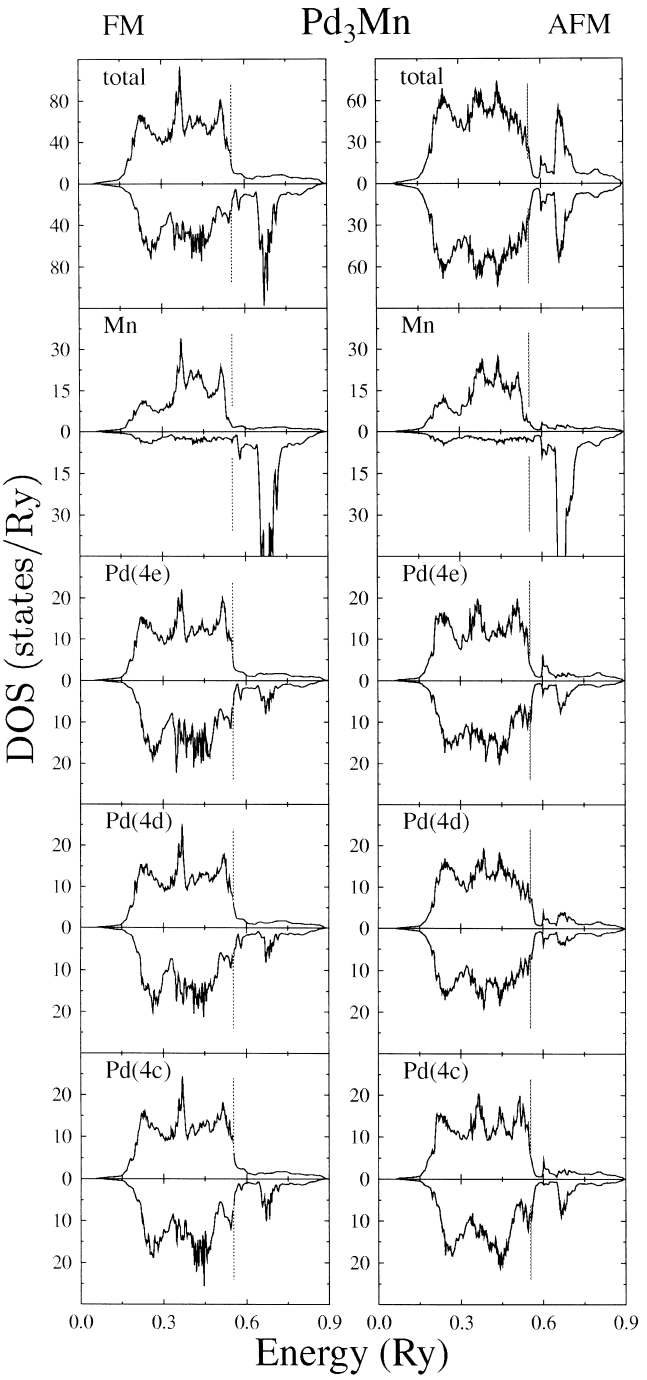

Fig. 5. Spin-polarised total and site-decomposed KKR DOS in the Pd_3Mn antiphase (FM, ferromagnetic; AFM, antiferromagnetic). A vertical line marks E_F.

neutron diffraction studies in Pd_3Mn (4.0 μ_B, 0.2 μ_B [1] and 4.1 μ_B, 0.15 μ_B [14]). However, later experimental studies have detected more complex magnetic structures in this compound [15].

Pd_3V in the considered structures is found near the magnetic instability, according to an analysis of $E_{tot}(a)$ and non-polarised DOS spectra (Fig. 4). In the $L1_2$ phase of Pd_3V, electronic bands split upon inclusion of the spin-polarisation due to a large *d*-DOS at E_F on V (Fig. 4), resulting in a total magnetic moment of 1.29 μ_B ($\mu_V = 1.34$ μ_B, $\mu_{Pd} = -0.03$ μ_B). Conversely, in the tetragonal body-centred phase of Pd_3V, rather low non-polarised DOS at E_F (Fig. 3) gives a non-magnetic ground state.

The KKR calculations in Pd_3Fe show that magnetic properties should appear both in $L1_2$ and DO_{22} structures, with the total magnetic moments: 4.09 μ_B and 3.93 μ_B, respectively.

The local magnetic moments in the DO_{22} of Pd_3Fe are found (in μ_B) 3.21, 0.21 and 0.27, on Fe, Pd (2*b*) and Pd (4*d*), respectively. The values are rather close to those calculated in the $L1_2$ phase: 3.25 μ_B (Fe) and 0.29 μ_B (Pd). As Pd in $L1_2$ and Pd (4*d*) in DO_{22} have the same next nearest atomic neighbours, the close values of the respective magnetic moments are calculated.

References

[1] J.W. Cable, E.O. Wollan, W.C. Koehler, H.R. Child, Phys. Rev. 128 (1962) 2118.
[2] H. Sato, R.S. Toth, Phys. Rev. 139 (1965) 1581.
[3] A.E. Carlsson, P.J. Meschter, J. Mater. Res. 4 (1989) 1060.
[4] J. Xu, A.J. Freeman, Phys. Rev. B 40 (1989) 11927.
[5] S. Jaswal, Solid State Common. 52 (1984) 127.
[6] T. Nautiyal, S. Auluck, J. Phys. Condens. Matter 1 (1989) 2211.
[7] Z.W. Lu, B.M. Klein, A. Zunger, Phys. Rev. Lett. 75 (1995) 1320.
[8] C. Wolverton, A. Zunger, Phys. Rev. B 52 (1995) 8814.
[9] S. Kaprzyk, Acta Phys. Pol. A 91 (1997) 135.
[10] A. Bansil, S. Kaprzyk, P.E. Mijnarends, J. Tobola, Phys. Rev. B 60 (1999) 13396.
[11] P. Villars, L.D. Calvert, Pearson's Handbook of Crystallographic Data for Intermetallic Phases, ASM, Metals Park, OH, 1991.
[12] U. von Barth, L. Hedin, J. Phys. C 5 (1972) 1629.
[13] S. Kaprzyk, P.E. Mijnarends, J. Phys. C 19 (1986) 1283.
[14] E. Kren, G. Kadar, M. Marton, Solid State Commun. 10 (1972) 1195.
[15] P. Onnerud, Y. Andersson, R. Tellgren, P. Nordblad, J. Solid State Chem. 128 (1997) 109.